Acoustics 2021
Wollongong, Australia
MAKING WAVES

An experimental investigation of the flow field and noise generation at a NACA 0012 wingtip

T. Zhang, Y. Ding, J. Fischer, Y. Yauwenas, C. de Silva, C. Doolan and D. Moreau

School of Mechanical and Manufacturing Engineering, UNSW Sydney, Australia

ABSTRACT

This paper presents an experimental investigation of the tip vortex formation noise produced by a wall-mounted finite airfoil. To characterise the noise at the wingtip, acoustic measurements taken in the UNSW open jet anechoic wind tunnel with a planar microphone array are presented for a NACA 0012 airfoil with varying aspect ratios at different geometric angles of attack and chord-based Reynolds numbers. Measurements of the mean streamwise total pressure field at the wingtip using a single pitot probe for selected test cases are included to link the flow dynamics with noise production. Furthermore, the flow interaction between the wingtip and the wing-wall junction region and its effect on tip noise generation for a low aspect ratio ($AR = 0.2$) NACA 0012 airfoil will also be examined.

1 INTRODUCTION

The vortex formed at the tip (or free end) of a wall-mounted finite airfoil can be a significant source of flow-induced noise for aircraft airframe components, wind turbine blades and submarine rudders. Understanding the nature of the tip noise mechanism and vortex formation process is a necessary precursor to understanding the connection between the fluid mechanics and the acoustics towards developing low noise tip devices for practical applications. While there have been some studies that investigate tip vortex flow (Birch and Lee, 2005; Karakus, Akilli and Sahin, 2008; Giuni and Green, 2013), only a few have explored tip noise generation (Brooks and Marcolini, 1986; Moreau and Doolan, 2016), which is the main topic of this paper.

Airfoil tip vortices are formed due to the pressure difference between the airfoil's pressure side and sunction side accompanied by the roll-up of the shear layer shed from the wingtip and the streamwise velocity component (Giuni and Green, 2013). Tip vortex formation noise is associated with the high level of turbulence over the wingtip and the trailing edge-tip region, as shown in Figure 1. It manifests itself as a peak in the airfoil noise spectrum that increases in amplitude with the angle of attack, Reynolds number and surface roughness due to a change in the aerodynamic and airfoil boundary layer properties (Brooks and Humphreys, 2003). George et al. (1980) were one of the first to experimentally investigate the mechanism of airfoil tip noise. They developed a semi-empirical noise model using a dipole approximation to model the trailing edge interaction of the separated flow region over the flat tip. Brooks and Marcolini (1986) improved upon George et al.'s prediction model using their measurements of tip vortex noise (Brooks and Marcolini, 1986). Single-point microphone measurements were taken on a NACA 0012 airfoil with a rounded tip and an aspect ratio of AR = 1-6 at a Reynolds number of Re = 80k to 100k, based on chord. They isolated the tip noise produced by the three-dimensional airfoils by comparing the noise to that of their two-dimensional counterparts. The model was then further modified by Brooks et al. (1989) to include the case of an airfoil with a flat tip, developed as part of their famous semi-empirical model (the so-called BPM model). Klei et al. (2014) examined the effect of elliptical rounding of the wingtip on the noise generation using an unswept Clark-Y airfoil with $AR = 5$ at Reynolds numbers up to Re = 120k. This study showed that the elliptical rounding increases the frequency of the peak noise as angles of attack increases, while the non-elliptical reference case showed that the peak frequency scales inversely with the angle of attack, due to the different noise generation mechanisms. More recently, Moreau and Doolan systematically investigated the acoustic signature of three-dimensional airfoils with flat tip (Moreau and Doolan, 2016; Moreau et al., 2016). In their studies, a planar microphone array was employed, and a NACA 0012 airfoil with an aspect ratio of AR = 1-3 was tested at a range of Reynolds numbers (Re = 790k to 1600k) and angles of attack (α = 0° to 12°). The studies revealed that the BPM model underpredicted the tip noise, especially at high frequencies, and a new flat-tip empirical noise prediction model incorporating the effective angle of attack at the airfoil tip based on Prandtl's lifting line theory was proposed. Zhang et al. (2021) investigated the effects of the airfoil profile and tip geometry on the tip noise signature. A critical frequency was discovered to distinguish the effect of the thickness of the airfoil on the noise spectra. Above the critical frequency, a thicker airfoil produces a lower amplitude tip noise peak, especially at mid-to-high frequencies above 5 kHz. An increase in the surface curvature of the airfoil was found to increase the tip noise level, especially for frequencies over 3 kHz and high angles of attack. Further, the presence of a rounded tip was found to be effective in the tip noise reduction by up to 5.6 dB over the frequency range of 5-15 kHz.

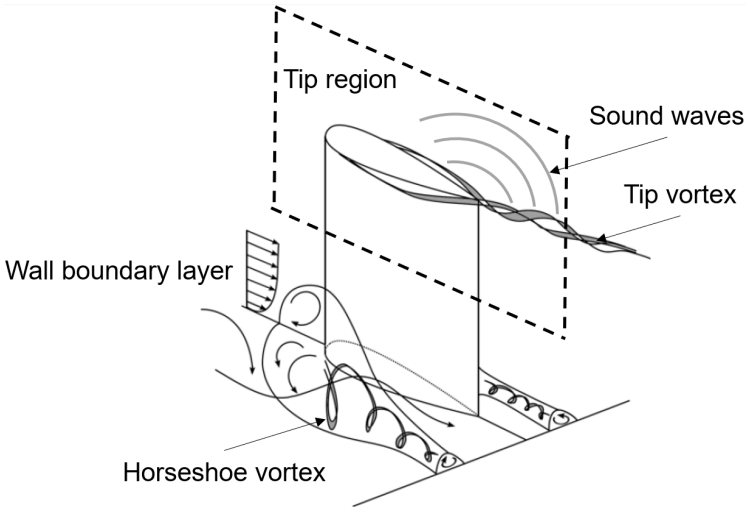

Figure 1: A schematic diagram of the flow structures around a wall-mounted airfoil. The focus of this study is the sound waves generated in the tip region (shown in the black dashed box). Figure adapted with permission from Moreau and Geyer (2021).

One aspect of airfoil tip noise generation that remains univestigated is the effect of airfoil aspect ratio on the tip flow structure and noise production. In particular, information at low aspect ratio, where the wall boundary layer and junction flow can significantly affect the tip flow and its induced noise, is scarce. As such, this paper presents an experimental investigation of the tip vortex formation noise produced by a wall-mounted finite airfoil focusing on the impact of the airfoil aspect ratio. To characterise the noise at the wingtip, acoustic measurements have been taken in the UNSW anechoic wind tunnel with a planar microphone array for a NACA 0012 airfoil with varying aspect ratios ($AR = 0.2$, 0.5 and 1) at different geometric angles of attack ($\alpha = 0°$ to 15°) and chord-based Reynolds numbers ($Re = 150$k to 600k). To explore the flow field at the wingtip responsible for noise generation, measurements of the mean streamwise total pressure field about the wingtip for a selected test case have been taken. Specifically, the flow interaction between the wingtip and the wing-wall junction region and its effect on tip noise generation for a low aspect ratio ($AR = 0.2$) NACA 0012 airfoil is investigated.

2 METHODOLOGY

The methodology involves two experimental campaigns. The first is the acoustic measurements taken for NACA 0012 airfoils with variations in aspect ratio, Reynolds number and angle of attack. The second campaign is a flow experiment performed for the low aspect ratio ($\mathrm{AR} = 0.2$) NACA 0012 at $\alpha = 10°$. Both experiments were performed in the acoustic tunnel at UNSW Sydney, Australia. The UNSW acoustic wind tunnel (UAT) is an open-jet anechoic wind tunnel that features a test section inside of a $3 \times 4.6 \times 2.15$ m^3 chamber with Basotect acoustic foam on every interior surface to produce a quasi-anechoic environment. The test section outlet has a cross-section of 0.455×0.455 m^2, and all the test models were mounted onto a circular turntable located within a side plate attached to the wind tunnel outlet (see Figure 2(a)). The turntable allows altering the geometric angle of attack by rotating the airfoil-turntable rig based on the angle indicator shown in Figure 2(a). The maximum turbulence intensity of the UAT is less than 1% at the flow speed of $\mathrm{U}_\infty = 45$ m/s, corresponding to a Reynolds number of $\mathrm{Re} = 600$k in this study. A complete description of the UAT can be found in Doolan et al. (2018). The two experimental campaigns utilised the same airfoil test models. These were manufactured from aluminium with a NACA 0012 profile and a flat tip. The airfoils had a chord length of 0.2 m and a span of 0.04, 0.1 and 0.2 m corresponding to an aspect ratio of $\mathrm{AR} = 0.2$, 0.5 and 1, respectively. Trip tape with a zig-zag profile and a thickness of 0.6 mm was applied to both sides of the airfoil at 10% chord to suppress the high-amplitude tones associated with laminar boundary layer instabilities (Zhang et al., 2020).

2.1 Acoustic Measurements

Acoustic measurements were taken for all three airfoil models with different aspect ratios at various geometric angles of attack ($\alpha = 0°$, 5°, 10° and 15°) and Reynolds numbers ($Re = 150$k, 275k, 400k to 600k), based on chord. Far-field acoustic data were obtained using a planar microphone array containing 64 GRAS type ¼ inch microphones with a flat frequency response of up to 20 kHz. The array was installed on the suction side of the airfoil, as shown in Figure 2(a). Each individual microphone was arranged in an optimised spiral pattern to have the smallest beamwidth but the largest aperture (Dougherty, 1998; Underbrink, 2002; Jiang et al., 2021). A Cartesian coordinate system is defined such that its origin is located at the leading edge-junction of the airfoil. The

streamwise direction was oriented along the positive x axis, while the spanwise direction was along the positive z axis. The centre microphone of the array was located 0.12 m upstream from the airfoil trailing edge, 0.32 m above the wingtip and 1.14 m away from the airfoil chord line when the $AR = 1$ airfoil is at zero angle of attack. The acoustic signals from the microphone array were acquired using a National Instruments PXI platform with a 24-bit resolution at a sampling rate of 51.2 kHz for 32 s. Sound maps were obtained by creating the cross-spectral matrix and then deconvoluted using the CLEAN-SC algorithm to remove the influence of the point spread function (Sijtsma, 2007) with a type IV steering vector formulation (Sarradj, 2012). The size of the scanning grid is 1.5×1.5 m^2 with a resolution of 0.01 m. The sound maps are displayed in 1/3rd octave bands. In addition to the sound pressure map distributions, 1/3rd octave band tip noise spectra were also obtained by integrating over the tip region for different airfoils, as shown in Figure 3. A fixed-size integration region was defined for all three airfoil models based on the inspection of the sound maps to ensure that all noise sources at the wingtip had been captured sufficiently. All 1/3rd octave band noise spectra and beamforming maps presented in this paper are in dB, relative to 20 μPa.

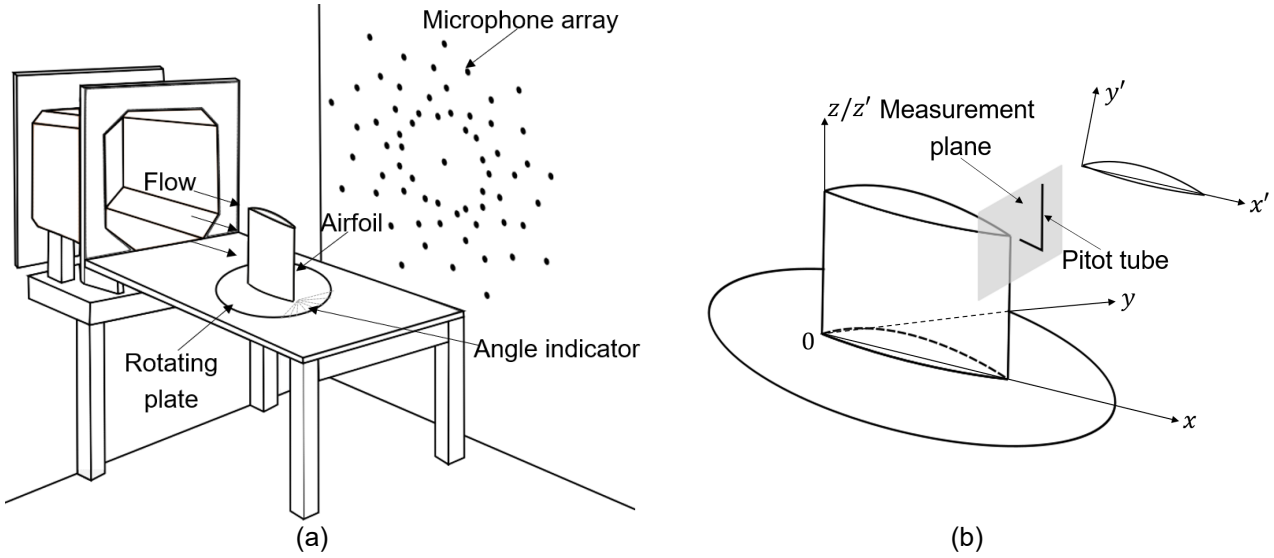

Figure 2: Experimental set-up for the measurements in the UAT. Schematic for (a) the acoustic measurements and (b) flow measurements.

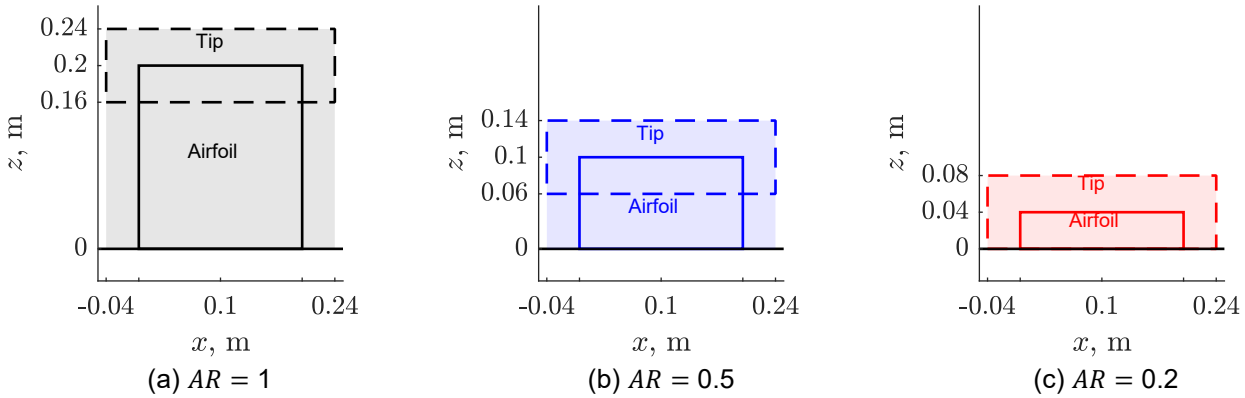

Figure 3: Integration regions for different airfoil models. The dashed box represents the integration area at the tip, and the shaded region shows the integration region for the whole airfoil. The flow is from left to right, and the junction of airfoils are all located at $z = 0$ m.

2.2 Flow Field Measurements

Flow measurements were conducted for the shortest airfoil ($AR = 0.2$) at $\alpha = 10°$ and a Reynolds number of $Re = 275$k, based on chord. The pressure field encompassing the whole airfoil region was obtained with a flattened L-shaped pitot probe with an inner diameter of 0.4 mm. The pitot probe was mounted on a 3D printed arm supported by a Dantec Dynamic three-axis traverse system, allowing data acquisition on different downstream measurement planes. The pressure signals were acquired with a Scanivalve DSA 2317 pressure scanner. New

sets of coordinate systems are defined in Figure 2(b) such that the flow-fixed coordinate system (x', y' and z') and the body-fixed coordinate system (x, y and z) share the same origin at the leading edge-junction of the airfoil and the same wall-normal axis z or z'. The (x', y', z') system is fixed and the (x, y, z) system follows rotational transformation based on the geometric angle of attack. Spanwise-wall normal planes of mean velocity were measured with the model in place at four different streamwise locations of $x'/c = 0.3$, 0.5, 0.8 and 1.02. Each plane has 2480 testing points over a 40 × 62 grid with a maximum spacing of 1 mm on the $y' - z'$ plane to obtain good resolution. The surface curvature of the airfoil causes an offset between the pitot tube and the pressure surface at each location during data acquisition on the pressure side of the airfoil. This offset value is stated in Table 1. Pressure measurements were taken on the pressure side, suction side, and tip region separately and then combined to build the entire streamwise pressure field. The pressure field data presented in this paper is the streamwise component due to the airfoil model's surface curvature and the flow's three-dimensionality. The non-dimensional streamwise pressure coefficient $Cp_0 = (p_{pitot} - p_{static})/p_{dynamic}$, where p_{pitot} is the total pressure from the pitot probe; p_{static} is the static pressure in the free stream; and $p_{dynamic}$ is the dynamic pressure in the free stream.

Table 1: The offset of the pitot tube on the pressure side at different streamwise locations.

	$\alpha = 10°$
$x'/c = 0.3$	4.4 mm
$x'/c = 0.5$	2.3 mm
$x'/c = 0.8$	1.6 mm

3 RESULTS

3.1 Acoustic Results

To illustrate the tip noise source strength and location, sound maps for the NACA 0012 airfoil with three different aspect ratios at $\alpha = 10°$ and the highest Reynolds number of $Re = 600$k are presented in Figure 4. The sound maps are shown at the selected 1/3rd octave band centre frequency of 4 kHz, corresponding to a Strouhal number of $St_c = f \cdot c/U_\infty = 18$, based on chord c. The sound maps of Figure 4 are in agreement with previous studies (Moreau et al., 2016; Zhang et al., 2021), which show the dominant noise source moves towards the trailing edge-tip of the airfoil as the angle of attack increases, especially at mid-to-high frequencies above 2−3 kHz. They also aid in determining the tip integration region, as shown in Figure 3. The sound maps for all three models show that the trailing edge part of the wingtip is the dominant noise source (at specific frequencies) under this flow condition, and the size of the source region in both streamwise and spanwise directions is similar. For the $AR = 0.2$ airfoil, the tip source extends down to the wing-wall junction encompassing the whole trailing edge. The peak noise level of the tip noise source is observed to decrease as the aspect ratio decreases, from 51 dB to 46 dB and 38 dB for Figure 4(a-c), respectively.

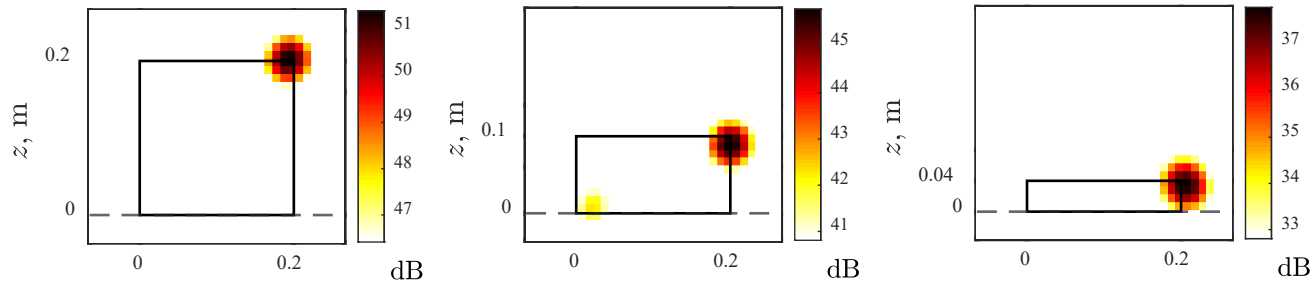

(a) $AR = 1$ (b) $AR = 0.5$ (c) $AR = 0.2$

Figure 4: One-third octave band beamforming maps processed using CLEAN-SC for NACA 0012 airfoils at $\alpha = 10°$, $Re = 600$k and a frequency of $f = 4$ kHz (St_c =18) with an aspect ratio of (a) $AR = 1$, (b) $AR = 0.5$ and (c) $AR = 0.2$. The flow is from left to right, and the dashed line represents the rotating plate (note that the maximum value of each colour bar varies and the exact position of the trailing edge is 0.2 m × cos(10°) = 0.197 m).

Figure 5 shows the contribution of the tip noise to the total wall-mounted airfoil (WMA) noise produced by the $AR = 1$ and 0.5 airfoils at $\alpha = 10°$ and $Re = 600$k. The spectra for the $AR = 0.2$ case are not included due to the same integration region for the tip and the whole airfoil (the dashed box overlaps with the red shaded region shown in Figure 3(c)). The tip noise spectra feature a broad peak with frequency and corresponding Strouhal

number that remains the same for different aspect ratios at $St_C = 12$. As the aspect ratio decreases, the contribution of the tip to airfoil noise production increases, especially at low Strouhal numbers ($St_C < 12$, corresponding to frequencies below 4 kHz), where junction noise has been reported to dominate (Ding et al., 2021). This could be due to the junction flow being modified by the tip flow at low aspect ratios.

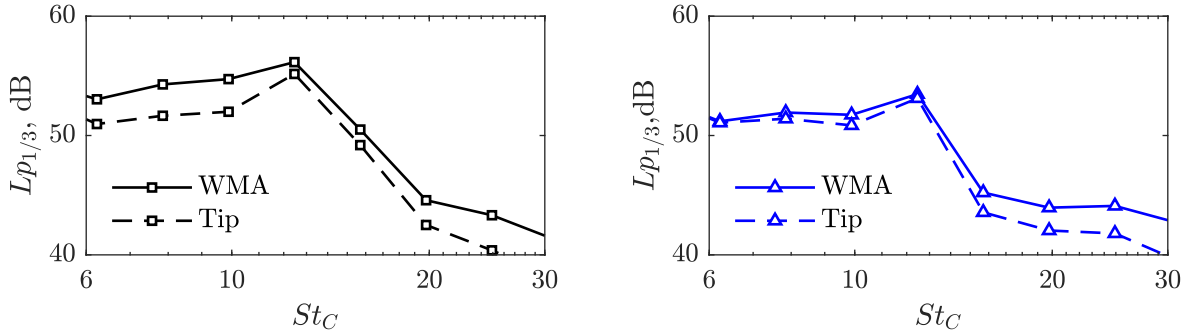

(a) $AR = 1$ (b) $AR = 0.5$

Figure 5: Comparison of the tip noise spectra to the total wall-mounted airfoil (WMA) noise spectra at $\alpha = 10°$, $Re = 600$k and (a) $AR = 1$ and (b) $AR = 0.5$.

Figures 6 and 7 show the effect of the angle of attack and the aspect ratio on the tip noise, respectively. The tip noise spectra were obtained by integrating the sound maps over the defined 2D regions (shown as the dashed box in Figure 3). A similar trend can be observed for the $AR = 1$ and 0.5 cases compared to $AR = 0.2$, as shown in Figure 6. The different acoustic behaviour of the lowest aspect ratio airfoil is likely due to the significant interaction between the tip and junction flows that impact the noise generation. Further, the tip integration region encompasses the entire airfoil for this lowest aspect ratio model. At $\alpha = 5°$ (see Figure 6(a)), the peak of the dominant tip noise source occurs at a Strouhal number of $St_C = 8$ for both $AR = 0.5$ and 1 airfoils. As the angle of attack increases (see Figure 6(b)), the peak Strouhal number also increases to $St_C = 12$, however the peak noise level decreases by about 3 dB. For the $AR = 0.2$ airfoil at the same Reynolds number, the tip noise peak is located at Strouhal number of $St_C = 10$ regardless of the angle of attack. More interestingly, a sudden drop in the tip noise can be observed at around $St_C = 15$, corresponding to a frequency of 3.5 kHz for the $AR = 0.2$ case, while a slightly smaller dip at the same frequency is shown in the $AR = 0.5$ case. In the mid-frequency range of $12.5 < St_C < 20$ (corresponding to frequencies between 3 kHz to 5 kHz), the noise levels of the two longer airfoils deviates up to 4 dB and 6 dB at $\alpha = 5°$ and 10°, respectively, suggesting that the effect of the mid-span flow is high. However, the noise level for the $AR = 0.5$ case is higher than the $AR = 1$ above $St_C = 20$ (5 kHz), and this could be due to the increased size of the integration region (as a percentage of airfoil span) and the effect of the combined trailing edge and tip flow on the noise generation.

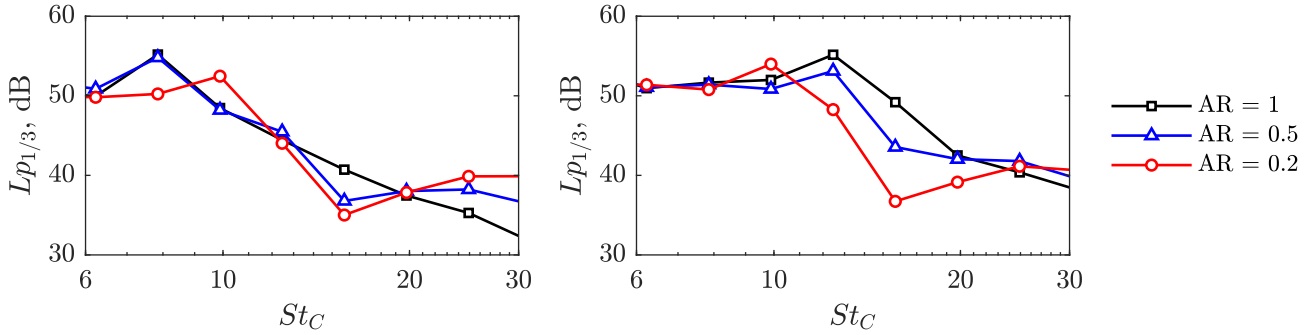

(a) $Re = 600$k, $\alpha = 5°$ (b) $Re = 600$k, $\alpha = 10°$

Figure 6: Tip noise spectra for airfoils with different aspect ratios at $Re = 600$k and (a) $\alpha = 5°$ and (b) $\alpha = 10°$.

At low Reynolds numbers, the effect of the angle of attack with variation in aspect ratio on the tip noise is small at low angles of attack (see $\alpha = 0°$ and 5° in Figure 7(a-b)). However, the peak noise level increases up to 6.6 dB for the $AR = 1$ case at $St_C = 13.6$, and 4 dB for the $AR = 0.2$ case at $St_C = 10.8$ at $\alpha = 10°$. A further increase in α to 15° does not affect the frequency of the noise tip peak for both aspect ratios, but an increase in the noise

level up to 5.3 dB can be observed for $AR = 1$ case, while the $AR = 0.2$ case remains stable. At the higher flow speed shown in Figure 7(c-d), the acoustic behaviour is different to $Re = 275$k. For $AR = 1$, the sudden change in the frequency and amplitude of the tip noise peak from $\alpha = 5°$ to 10° can be due to a large increase in the magnitude of the vorticity at the tip. This is confirmed by Igarashi et al., who investigated the evolution of the tip vortex with varying angles of attack using Stereoscopic Particle Image Velocimetry (Igarashi et al., 2010), a non-intrusive laser optical measurement technique for measuring the three-dimensional velocity field within the flow. Another reason could be due to the different characteristics of the tip vortex at these two angles of attack (Awasthi et al., 2018). Increasing the angle of attack for $AR = 0.2$ only slightly affects the tip noise level and the spectral trend. This can be due to the decreased sensitivity of the low aspect ratio airfoil to the change in the tangential velocity and the vorticity at different angles of attack due to a lower effective angle of attack at the tip. Another reason can be the integration region, which encompasses the entire airfoil for this aspect ratio thus capturing the combined impact of junction, trailing edge and tip flow.

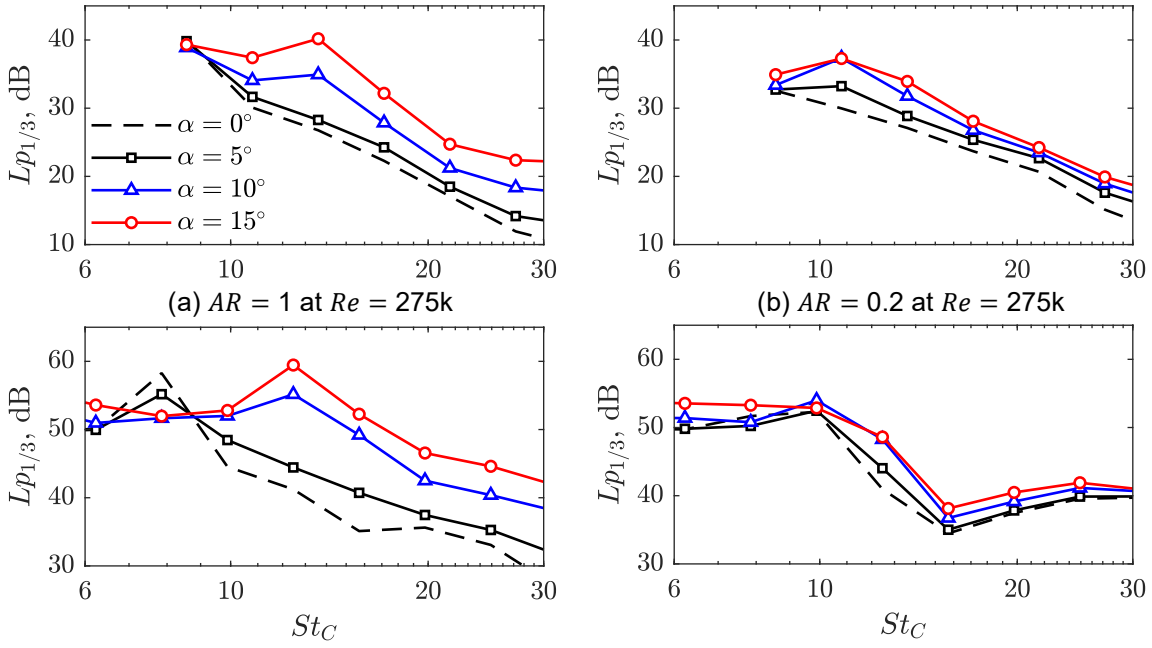

(a) $AR = 1$ at $Re = 275$k (b) $AR = 0.2$ at $Re = 275$k

(c) $AR = 1$ at $Re = 600$k (d) $AR = 0.2$ at $Re = 600$k

Figure 7: Tip noise spectra for $AR = 1$ (first column) and 0.2 (second column) airfoils at different α and Re. Please note that there are no results shown at $St_C < 8$ in (a) and (b) due to the frequency limit at low Reynolds number.

3.2 Pressure Field Results

Figure 8 shows contour maps of the streamwise total pressure coefficient distribution at $\alpha = 10°$ and a Reynolds number of $Re = 275$k for the $AR = 0.2$ airfoil. The black region in the contour plots represents the projection of the airfoil on the $y' - z'$ plane, while the open region represents the gap between the pitot probe and the surface of the airfoil, where the offset is listed in Table 1. A linear interpolation method was applied to the measurement points to generate continuous contour levels. The tip vortex structure can be clearly seen in Figure 8. The pressure loss shown in the figure is caused by the vortex structures within the field of view. At $x/c = 0.3$ and 0.5 (see Figure 8(a-b)), the flow separates and forms a vortex on the pressure surface-tip edge (at $y' < 0$) when it encounters the sharp edge of the tip. The strength of this vortex at the tip decreases as it moves downstream along the chord and the location of the vortex centre (the local minimum Cp_0 over the tip in the contour plots) lifts and stretches towards the suction surface-tip sharp edge. Another vortex lies on the suction surface-tip sharp edge on the suction side, where $y' > 0$. Moving along the chord to $x/c = 0.8$ (Figure 8(c)), the vortex on the suction side grows in size and begins to detach from the surface. From $x/c = 0.3$ to 0.8, the tip vortex system extends from the tip to the inboard region of the wing surface up to $z/s = 0.7$, corresponding to 12 mm from the wingtip towards the wing-wall junction. Due to the pressure difference between the pressure side and the suction side, the tip-surface vortex that originated on the pressure side is entrained into the main vortex structure on the suction side at $x/c = 0.8$. The trailing tip vortex phenomenon is observed at $x/c = 1.02$ (in Figure 8(d)), where a symmetric vortex extends to $z/s = 0.5$, corresponding to 20 mm from the suction tip edge towards the junction.

In addition to the tip vortex formation, the interaction between the tip and the junction flow can also be observed in Figure 8. This is especially evident when comparing the results of Figure 8 to the authors' previous junction flow measurements taken on the $AR = 1$ airfoil (Ding et al., 2021). The effect of the tip vortex on the flow field is different on the suction side and pressure side depending on the aspect ratio. When comparing the total streamwise pressure coefficient for $AR = 1$ from the previous study (Ding et al., 2021) with $AR = 0.2$ from this study at the same flow condition (α =10° and $R_e =$ 275k), the roll up of the horseshoe vortex at the junction on the suction side is weakened, while the vortex on the pressure side is strengthened for the lower AR case. In Figure 8, the shear layer on the suction side of the airfoil surface is thicker from the junction to the mid-span region ($0 < z/s < 0.5$) along the chord. A valley forms between the suction side-tip surface vortex and the shear layer at $x/c = 0.3$ and 0.5 and is then replaced with a more developed primary vortex at $x/c = 0.8$. Compared with the $AR = 1$ case, the depth of the valley and the downwash effect are reduced as the aspect ratio decreases. Moving further downstream ($x/c = 1.02$), the tip vortex core grows and stretches towards to wall, further modifying the junction vortex structure and the shear layer on the surface of the airfoil. Different from the downwash effect, the upwash effect at the junction appears to be stronger for the $AR = 0.2$ case. The different pressure fields for these two aspect ratios are due to the interaction between the tip and junction flows, especially at $x/c = 1.02$ as the size of the tip vortex grows and stretches towards the wall.

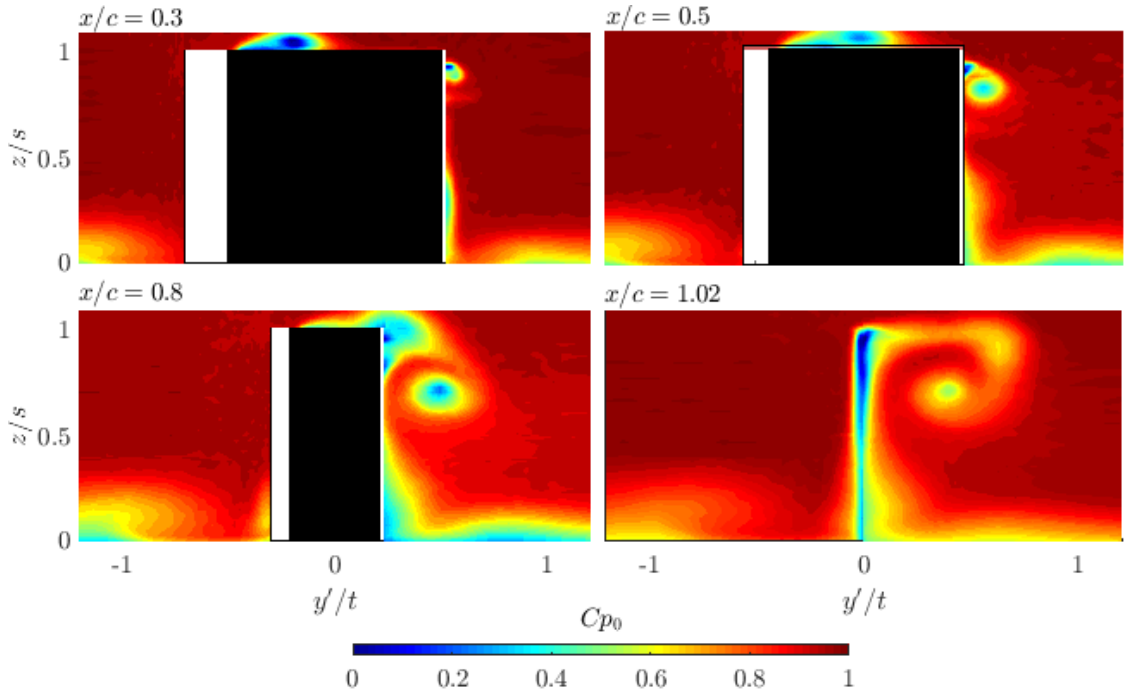

Figure 8: Contours of streamwise total pressure coefficient for a NACA 0012 airfoil with $AR = 0.2$ at $\alpha =$ 10°, $Re =$ 275k and various downstream locations of $x/c = 0.3$, 0.5, 0.8 and 1.02. Note that the flow is out of the plane of the page. The pressure side has $y' < 0$, and c, s and t represent the airfoil chord length, span and maximum thickness, respectively.The black regions represent the cross-section area of the airfoil and the open regions represent the gap between the ptitot probe and the airfoil due to the surface curvature. In addition, the particular figure aspect ratio was selected to enhance the vortex features.

4 CONCLUSION

This study examined the tip noise generation and vortex characteristics for NACA 0012 airfoil models with different aspect ratios through two sets of experimental campaigns in an anechoic wind tunnel at UNSW. The noise measurements showed that the wingtip is a dominant noise source, especially at mid to high frequencies above 2-3 kHz for all the airfoil models. As the aspect ratio decreases, the effect of the tip noise on the whole airfoil acoustic signature is more prominent even at lower frequencies due to the junction flow being modified by the tip vortex. The frequency of the peak noise remains fixed with aspect ratio, but the magnitude scales with the aspect ratio. At low Reynolds numbers, the effect of the aspect ratio is not apparent, and an increase in the angle of attack leads to a higher noise level. While at higher Reynolds numbers, the acoustic signature of lower and higher aspect ratio airfoils is different. The streamwise pressure measurements on the 0.2 aspect ratio airfoil clearly show the formation and development of the tip vortex. The presence of the primary and secondary vortex can be observed by identifying the local minima regions of the streamwise total pressure coefficient.

REFERENCES

Awasthi, M., Moreau, D. and Doolan, C. (2018) “Flow structure of a low aspect ratio wall-mounted airfoil operating in a low Reynolds number flow”, *Experimental Thermal and Fluid Science*, vol. 99, pp. 94–116. https://doi.org/10.1016/j.expthermflusci.2018.07.019

Birch, D. and Lee, T. (2005) “Investigation of the near-field tip vortex behind an oscillating wing”, *Journal of Fluid Mechanics*, vol. 544, pp. 201–241. https://doi.org/10.1017/S0022112005006804

Birch, D. and Lee, T. (2005) “Tip vortex behind a wing undergoing deep-stall oscillation”, *AIAA Journal*, vol. 43, pp. 2081–2092. https://doi.org/10.2514/1.13139

Brooks, T. and Marcolini, M. (1986) “Airfoil tip vortex formation noise”, *AIAA Journal*, vol. 24, pp. 246–252.

Brooks, T., Pope, D. and Marcolini, M. (1989) “Airfoil self-noise and prediction”, National Aeronautics and Space Administration. https://ntrs.nasa.gov/api/citations/19890016302/downloads/19890016302.pdf

Brooks, T. and Humphreys, W. (2003) “Flap-edge aeroacoustic measurements and predictions”, *Journal of Sound and Vibration*, vol. 261, pp. 31–74. https://doi.org/10.1016/S0022-460X(02)00939-2

Ding, Y., Zhang. T., Geyer, T., de Silva, C., Doolan, C. and Moreau, D. (2021) “Experimental investigation of the flow characteristics and noise generation at the wing–wall junction,” *Journal of Aerospace Engineering*, vol. 34, pp. 04021054. https://doi.org/10.1061/(ASCE)AS.1943-5525.0001303

Doolan, C., Awasthi, M., Moreau, D. and Jiang, C. (2018) “The UNSW anechoic wind tunnel”, *Proceedings of Acoustics 2018, Adelaide, Australia.*

Dougherty, R. (1998) “Spiral-shaped array for broadband imaging”. Pat. US 5,838,284.

George, A., Najjar, F. and Kim, Y. (1980) “Noise due to tip vortex formation on lifting rotors”, *Proceedings of AIAA 1980, Reston, Virigina.* https://doi.org/10.2514/6.1980-1010

Geyer, T. and Moreau D. (2021) “A study of the effect of airfoil thickness on the tonal noise generation of finite, wall-mounted airfoils”, *Aerospace Science and Technology*, vol. 115, pp. 106768 – 106768. http://dx.doi.org/10.1016/j.ast.2021.106768

Giuni, M. and Green, R. (2013) “Vortex formation on squared and rounded tip”, *Aerospace Science and Technology*, vol. 29, pp. 191–199. https://doi.org/10.1016/j.ast.2013.03.004

Igarashi, H., Durbin, P., Hu, H. and Ma, H. (2010) “A stereoscopic PIV study of a near-field wingtip vortex”, *Proceedings of AIAA 2010, Orlando, Florida.* https://doi.org/10.2514/6.2010-1029

Jiang, C., Moreau, D., C., Fischer, J. and Doolan, C. (2021) “Additively manufactured sound-absorbing porous structures for airfoil trailing-edge noise control”, *Journal of Aerospace Engineering*, vol. 34, pp. 04021068. https://doi.org/10.1061/(ASCE)AS.1943-5525.0001317

Karakus, C., Akilli, H. and Sahin, B. (2008) “Formation, structure, and development of near-field wing tip vortices”, *Proceedings of the Institution of Mechanical Engineers, Part G: Journal of Aerospace Engineering*, vol. 222, pp. 13–22. https://doi.org/10.1243/09544100JAERO274

Klei, C., Buffo, M., and Stumpf, E. (2014) “Effects of wing tip shaping on noise generation”, *Inter-noise 2014, Melbourne, Australia.*

Moreau, D. and Doolan, C. (2016) “Wall-mounted finite airfoil-noise production and prediction”, *AIAA Journal*, vol. 54, pp. 1637–1651. https://doi.org/10.2514/1.J054493

Moreau, D. and Doolan, C. (2016) “An experimental study of airfoil tip vortex formation noise”, *Proceedings of Acoustics 2016, Brisbane, Australia.*

Sarradj, E. (2012) “Three-dimensional acoustic source mapping with different beamforming steering vector formulations”, *Advances in Acoustics and Vibration*, vol. 2012, pp. 292695. https://doi.org/10.1155/2012/292695

Sijtsma, P. (2007) “CLEAN based on spatial source coherence”, *International Journal of Aeroacoustics*, vol. 6, pp. 357–374. https://doi.org/10.1260/147547207783359459

Underbrink, J. (2002) “Aeroacoustic phased array testing in low speed wind tunnels”. *Aeroacoustic Measurements*. Springer. Chap. 3, pp. 98–217. ISBN: 3-540-41757-5.

Zhang, T., Geyer, T., Fischer, J., Doolan, C. and Moreau, D. (2020) “Dataset on tip vortex formation noise produced by wall-mounted finite airfoils with flat and rounded tip geometries”, *Data in Brief*, vol. 28, pp. 105058. https://doi.org/10.1016/j.dib.2019.105058

Zhang, T., Geyer, T., de Silva, C., Fischer, J., Doolan, C. and Moreau, D. (2021) “Experimental investigation of tip vortex formation noise produced by wall-mounted finite airfoils”, *Journal of Aerospace Engineering*, vol. 34, pp. 04021079. https://doi.org/10.1061/(ASCE)AS.1943-5525.0001315